PAPER

Check for updates

Comparison of photoactivatable crosslinkers for in-gel immunoassays†

Kristine Y. Tan, [ID] [a] Surbhi Desai,[b] Erum Raja,[b] Chris Etienne,[b] Brian Webb[b] and Amy E. Herr [ID] *[a,c]

While fluorescence readout is a key detection modality for hydrogel-based immunoassays, background fluorescence due to autofluorescence or non-specific antibody interactions impairs the lower limit of detection of fluorescence immunoassays. Chemical modifications to the hydrogel structure impact autofluorescence and non-specific interactions. Benzophenone is a common photoactivatable molecule, and benzophenone methacrylamide (BPMA) has been used for cross-linking protein in polyacrylamide (PA) hydrogels. However, previous studies have suggested that the aromatic structure of benzophenone can contribute to increased autofluorescence and non-specific hydrophobic interactions with unbound fluorescent probes. Here, we synthesize diazirine methacrylamide (DZMA) as an alternative photoactivatable molecule to cross-link into PA hydrogels for in-gel protein capture for in-gel immunoassays. We hypothesize that the less hydrophobic structure of diazirine (based on previously reported predicted and experimental log P values) exhibits both reduced autofluorescence and non-specific hydrophobic interactions. We find that while equal concentrations of DZMA and BPMA result in lower protein target photocapture in the diazirine configuration, increasing the DZMA concentration up to 12 mM improves in-gel protein capture to be on par with previously reported and characterized 3 mM BPMA hydrogels. Furthermore, despite the higher concentration of diazirine, we observe negligible autofluorescence signal and a 50% reduction in immunoassay fluorescence background signal in diazirine gels compared to BPMA gels resulting in comparable signal-to-noise ratios (SNR) of the probed protein target. Finally, we test the utility of DZMA for single-cell immunoblotting in an open microfluidic device and find that protein migrates ~1.3× faster in DZMA hydrogels than in BPMA hydrogels. However, in DZMA hydrogels we detect only 15% of the protein signal compared to BPMA hydrogels suggesting that the diazirine chemistry results in greater protein losses following electrophoretic separations. We establish that while diazirine has lower background fluorescence signal, which may potentially improve immunoassay performance, the lower capture efficiency of diazirine reduces its utility in open microfluidic systems susceptible to sample losses.

Introduction

Beyond drug delivery vehicles[1] and cell[2] and tissue engineering scaffolds,[3,4] functionalized hydrogels play an increasingly important role in measurement science. From biosensing[5] to protein microarrays,[6,7] immunoassays utilize hydrogel structures due to the higher capacity[8] and sensitivity of hydrogel-based protein chips compared to surface-based chips.[9] For

hydrogel-based immunoassays, proteins are immobilized in the hydrogel matrix for immunoprobing, often relying on fluorescence detection as the target signal read-out method.

When designing immunoassays with fluorescence detection, it is important to consider sources of background fluorescence that can obscure the target signal. Background can originate from instrumentation and environmental sources (*e.g.*, the excitation source, camera, or ambient light) as well as from the sample, which can include autofluorescence from the sample or hydrogel material, as well as fluorescence from non-specific antibody interactions.

Benzophenone is a photoactivatable molecule that has been utilized to crosslink protein into hydrogel matrices for immunoassays.[10] Upon UV activation, the benzophenone molecule is activated to a biradical, able to abstract hydrogens from nearby C–H bonds, such as those on the protein backbone, and recombine to form a covalent C–C bond.[11] To func-

[a]The UC Berkeley – UCSF Graduate Program in Bioengineering, 94720 Berkeley, CA, USA. E-mail: aeh@berkeley.edu
[b]Department of Research and Development, Thermo Fisher Scientific, Rockford, Illinois, USA
[c]Department of Bioengineering, University of California, Berkeley, 94720 Berkeley, CA, USA
†Electronic supplementary information (ESI) available. See DOI: 10.1039/d1an01309b

tionalize hydrogels with benzophenone, benzophenone methacrylamide (BPMA) has been previously synthesized and is incorporated into the hydrogel matrix during polymerization.[10] BPMA hydrogels have been used to perform in-gel immunoprobing of target antigens, including the probing step of single-cell immunoblotting following microscale protein separations.[12]

However, with BPMA hydrogels, background fluorescence must be considered as the aromatic structure of benzophenone contributes to increase fluorescence immunoassay background signal. First, the aromatic ring structure on benzophenone contains conjugated double bonds, resulting in fluorescence in the visible spectrum and is a source of autofluorescence in the hydrogel.[13] Second, upon photoactivation, a side product (benzopinacol) can be formed that also emits fluorescence.[11,13] Third, the hydrophobic aromatic ring structures of both benzophenone and benzopinacol may facilitate non-specific hydrophobic interactions[13] that lead to increased immunoassay background signal from non-specific retention of unbound fluorescent probes.[14]

To boost in-gel immunoassay performance by reducing fluorescence background signal, we consider diazirine as an alternative photoactivatable molecule for protein crosslinking. Diazirine is (1) more hydrophilic than benzophenone[15,16] and thus less likely to non-specifically interact with hydrophobic immunoprobes, and (2) lacks conjugated double bonds that emit photons in the visible spectra upon activation. The chemical structure of diazirine consists of a three-membered ring composed of two nitrogen atoms and one carbon atom. Upon UV activation (∼350 nm), the diazirine ring breaks, irreversibly releasing N_2 and forming a reactive carbene species that can insert into nearby C–H or heteroatom–H bonds to form a covalent bond.[17,18]

However, the highly reactive carbene species has a shorter half-life, in the pico- to nano-second range, compared to the benzophenone diradical half-life of 120 μs.[18] Furthermore, while any unbound benzophenone can be reactivated upon subsequent exposure to UV,[11] carbenes can be quenched by the surrounding solvent, resulting in lower protein target crosslinking efficiency compared to benzophenone.[17,19] We hypothesize that the hydrophilic structure of diazirine will allow a higher concentration diazirine to be solubilized in the hydrogel precursor to improve in-gel protein capture while the hydrophobic structure of benzophenone limits the concentration that can be solubilized in the hydrogel precursor.

Here, we seek to reduce in-gel fluorescence background signal utilizing diazirine functionalized to acrylamide, hypothesizing that diazirine exhibits both reduced autofluorescence and reduced non-specific hydrophobic interactions based on its chemical properties. We first synthesized diazirine methacrylamide (DZMA) to incorporate diazirine into polyacrylamide (PA) hydrogels. We then utilized hydrogels functionalized with varying concentrations of DZMA to determine the optimal concentration for comparable protein capture to previously reported and characterized benzophenone gels.[10] Next, we compared the background signal from non-specific anti-

body interactions and autofluorescence in diazirine and benzophenone functionalized hydrogels. Finally, we utilized DZMA hydrogels to quantify single-cell protein expression in an in-gel immunoassay and compared protein capture and signal-to-noise ratios of detected protein targets to BPMA hydrogels. Our findings indicate that initial results with diazirine demonstrated comparable signal-to-noise ratios with BPMA hydrogels due to lower background signal, however further investigation into diazirine chemistry may be necessary for its use to specific immunoassay applications.

Results and discussion

Comparing protein capture in BPMA and DZMA hydrogels

After synthesizing diazirine methacrylamide (DZMA) (Note 1 in ESI†), we incorporated varying concentrations of DZMA into the hydrogel precursor to measure protein capture. Due to the (1) shorter half-life of activated diazirine (ps–ns range) compared to activated benzophenone (80–120 μs),[18] (2) potential quenching of the diazirine reaction by water whereas benzophenone can be repeatedly reactivated,[18,20] and (3) formation of a relatively stable diazo isomer side product upon diazirine activation,[17] we hypothesize that in-gel protein capture will be lower with diazirine compared to benzophenone. However, due to lower hydrophobicity of diazirine molecules compared to benzophenone molecules (based on predicted and experimental log P values[15,16]) we hypothesize that a higher concentration of diazirine in the hydrogel precursor will increase the protein capture efficiency. However, because diazirines are known to serve as carbon radical traps,[21] higher concentrations of diazirine may trap radicals necessary for gel polymerization thus impeding the polymerization process which would limit the concentration of diazirine that can be incorporated into the hydrogel.

To assess protein-capture in DZMA gels, we labeled GFP protein with DyLight 633 (GFP*) to immobilize in the hydrogel. We utilized the signal from the small fluorophore label to quantify protein capture instead of relying on the native GFP fluorescence which is dependent on the 3D protein structure and may be disrupted during in-gel immobilization and alter fluorescence readout. For each gel condition, we incubated physically isolated regions of the gel with either GFP* protein solution or a blank 1× PBS solution (Fig. 1A). After exposing the gels to UV to activate protein crosslinking, we washed the gels to remove uncaptured GFP* before imaging on a microarray scanner to measure the DyLight 633 fluorescence signal. We quantified protein capture from gel regions incubated with GFP* protein (Protein ROI), using blank gel regions (Blank ROI) incubated with 1× PBS, for background subtraction:

$$\text{Protein Capture Signal} = \text{Fluorescence}_{\text{Protein ROI}} - \text{Fluorescence}_{\text{Blank ROI}}$$

When DZMA was added at the same concentration as previously reported BPMA gels (3 mM)[12,22] to the gel precursor,
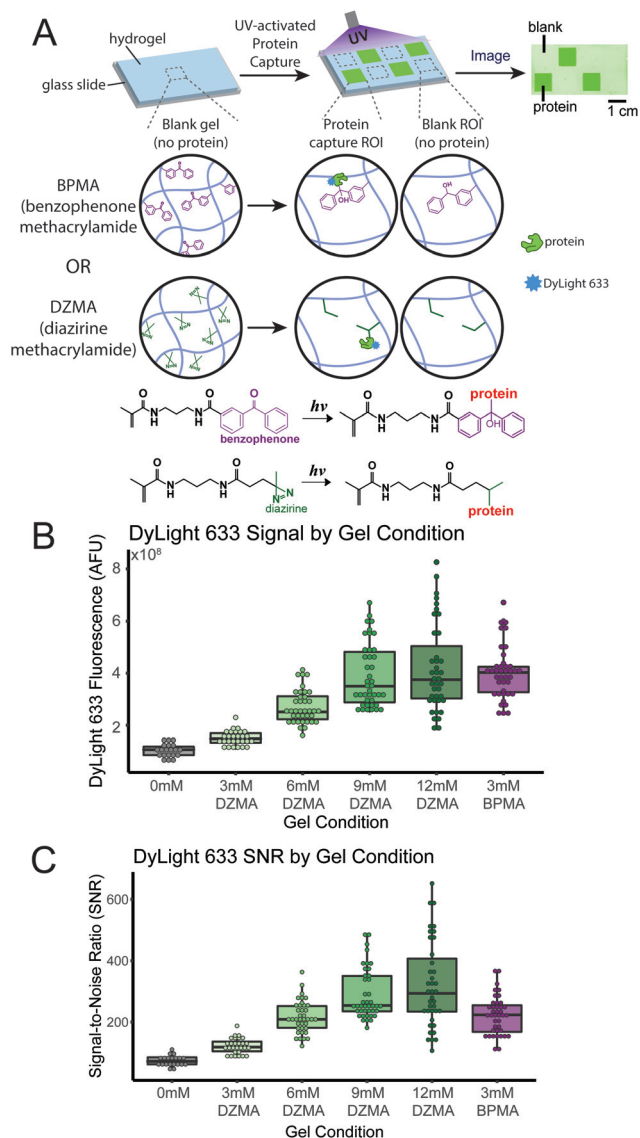
Fig. 1 In-gel protein capture of DyLight 633 labelled protein target in DZMA and BPMA functionalized hydrogels. (A) Schematic of hydrogels functionalized with BPMA or DZMA and protein capture. Hydrogels are fabricated with either BPMA or DZMA functional group. Specific regions of the gel are incubated with protein and protein capture is initiated by exposure to UV light. (B) Integrated fluorescence of protein regions in hydrogels with varying concentration of DZMA compared to 0 mM negative control and standard 3 mM BPMA gels. Integrated DyLight 633 signal increases as DZMA concentration increases, indicating greater protein capture at higher DZMA concentrations. N = 9–11 ROIs across 3 replicate devices per gel condition. (C) Corresponding signal-to-noise ratios of protein capture.

DZMA gels had significantly lower protein capture signal (Kruskal–Wallis with Holm correction, $p < 0.01$, n = 3 slides, 9–11 ROI regions) (Fig. 1B). We tested higher concentrations of diazirine due to our hypothesis that we could incorporate higher concentrations of the hydrophilic diazirine molecule into the gel to improve protein capture, increasing the concentration of DZMA up to 12 mM in the PA precursor. We

observed that increasing the concentration up to 12 mM resulted in comparable protein capture signal and higher signal-to-noise ratios (SNR) than the standard 3 mM BPMA gels. However, as we increased the concentration of DZMA, we observed that the time for hydrogel polymerization increased, despite using equivalent volume of the DMSO solvent.

Our results support our hypothesis that DZMA hydrogels have lower capture efficiency than BPMA hydrogels, evidenced by lower GFP* signal in 3 mM DZMA gels compared to the GFP* signal from the equivalent concentration 3 mM BPMA gels. However, by increasing the concentration of diazirine in the gel precursor, we were able to achieve greater protein capture compared to lower DZMA concentrations. The longer polymerization times associated with higher DZMA concentrations indicate that higher concentrations of photoactivatable molecules interfere with the hydrogel polymerization reaction, supporting that diazirines serve as carbon radical traps that interfere with hydrogel polymerization. Furthermore, if a portion of the diazirine molecules are quenched during gel polymerization, this could explain why we do not observe equal scaling between DZMA concentration and fluorescence signal, as well as why we observe a leveling off of signal at 9 mM and 12 mM DZMA.

Measuring sources of background in hydrogel-based immunoassays

Upon demonstrating that diazirine can be used for in-gel protein capture, we investigated the background signal from each functionalized hydrogel. We investigated background signal from each molecule due to (1) non-specific antibody retention in gels caused by any potential non-specific interactions between the functionalized gel matrix and antibody probe and (2) autofluorescence from the photoactive molecule itself. We hypothesize that the aromatic rings in benzophenone serve as a hydrophobic attraction force for immunoprobes to partition into the gel and be non-covalently retained in-gel. Furthermore, the conjugated double bonds in benzophenone result in fluorescence in the visible spectrum upon UV activation, contributing to gel autofluorescence.

To measure background fluorescence from non-specific immunoprobe retention, the same hydrogels with captured GFP* which were used to quantify protein capture in DZMA hydrogels and BPMA hydrogels were studied. Following UV protein capture, the gels were imaged before and after immunoprobing using the laser channel corresponding to the fluorescent immunoprobe (anti-GFP labelled with Alexa Fluor 555); thus measuring the fluorescence signal directly due to immunoprobe introduction.

To quantify the immunoprobed target signal (antibody binding to its protein target), we analyzed the GFP* protein regions in the gel after immunoprobing, using the adjacent non-protein blank regions of the gel after immunoprobing to
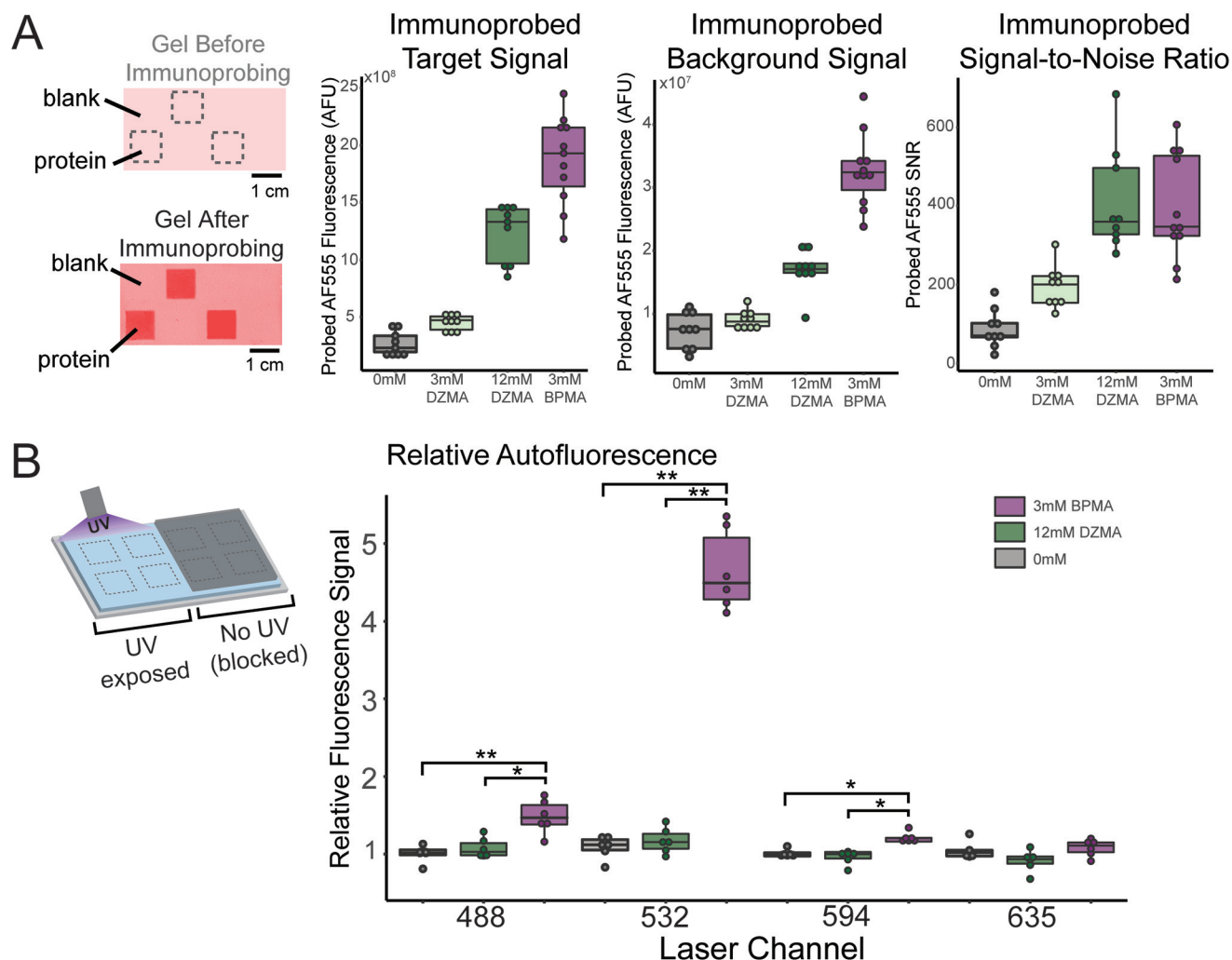
Fig. 2 Measuring sources that contribute to increased background fluorescence for in-gel immunoassays. (A) Analysis of the immunoprobed target from fluorescently labelled primary antibody in gel regions incubated with protein (Immunoprobed Target Signal) and blank (no protein) regions (Immunoprobed Background Signal), and corresponding SNR of Immunoprobed Target Signal. While Immunoprobed Target Signal is higher in 3 mM BPMA gels, Immunoprobed Background Signal which corresponds to non-specific antibody retention in the hydrogel is also higher, resulting in comparable SNR between 3 mM BPMA and 12 mM DZMA (n = 9–11 ROIs) (B) Analysis of relative background autofluorescence between 3 mM BPMA gels, 12 mM DZMA gels and blank (0 mM) negative control gels across four excitation laser channels in the microarray scanner. n = 6 ROIs, * p < 0.05; ** p < 0.01; Kruskal−Wallis with Holm multiple pairwise correction.

perform background subtraction. This background subtraction removes all background signal arising from both gel autofluorescence and non-specific antibody retention in the gel (Fig. 2A).

$$\text{Immunoprobed Target Signal}$$
$$= \text{Protein ROI}_{\text{probed}} - \text{Blank ROI}_{\text{probed}}$$

To specifically measure the background signal solely due to non-specific antibody interactions with the gel, we measured the fluorescence signal from the blank, non-protein regions, before and after immunoprobing. The signal from the blank regions before immunoprobing was used to mitigate contribution from gel autofluorescence and was subtracted from the

fluorescence signal after immunoprobing. Thus, the immunoprobe background signal only accounts for antibody signal in the gel that is not specifically bound to any protein target (Fig. 2A).

$$\text{Immunoprobed Background Signal}$$
$$= \text{Blank ROI}_{\text{after immunoprobing}} - \text{Blank ROI}_{\text{before immunoprobing}}$$

To quantify the autofluorescence background signal between DZMA and BPMA, we fabricated negative control gels, 12 mM DZMA gels, and 3 mM BPMA gels, and only activated half of the gel with UV light (Fig. 2B). We compared the fluorescence signal across the 4 laser channels (488, 532, 594, and 635 nm) of the microarray scanner. We quantified relative

autofluorescence as the fluorescence signal from the UV-activated gel normalized by the intensity of the non-activated gel.

$$\text{Relative Autofluorescence} = \frac{\text{Blank ROI}_{\text{UV-activated}}}{\text{Blank ROI}_{\text{non-activated}}}$$

Compared to 12 mM DZMA gels, 3 mM BPMA gels had significantly higher ($\sim$1.5$\times$) immunoprobed target signal (Kruskal–Wallis test with Holm pairwise correction, $p < 0.01$, $n = 9$–11 Protein ROIs) (Fig. 2A), and $\sim$1.9$\times$ higher immunoprobed background signal (Kruskal–Wallis test with Holm pairwise correction, $p < 0.01$, $n = 9$–11 Blank ROIs). Despite lower immunoprobed target signal in the 12 mM DZMA gels, the SNR of the probed protein target was comparable with the SNR in the 3 mM BPMA gels (Kruskal–Wallis test with Holm pairwise correction, $p = 1.0$, $n = 9$–11 Protein ROIs). Blank UV-activated BPMA hydrogels also emitted significant relative autofluorescence compared to negative control gels (Kruskal–Wallis with Holm pairwise correction, $p < 0.01$, $n = 6$ ROIs) (Fig. 2B), particularly in the 488 and 532 nm laser channels, having $\sim$1.5$\times$ and $\sim$4.7$\times$ the relative autofluorescence signal as non-UV-activated BPMA gels, respectively. In contrast, across all laser channels, UV-activated DZMA gels had 0.9$\times$–1.2$\times$ the relative autofluorescence signal of non-activated DZMA gels, comparable to the vehicle control gels ($p > 0.05$, Kruskal–Wallis test with Holm pairwise correction).

The higher immunoprobed background signal in 3 mM BPMA gels indicates more non-specific interactions retaining probe in the BPMA gels than in DZMA gels, supporting our hypothesis that the aromatic rings in benzophenone are a source of hydrophobic attraction that retain immunoprobes in the gel. As a result, the higher immunoprobed background signal in BPMA gels adversely affected the SNR of the immunoprobed target signal such that SNR was comparable between 12 mM DZMA gels and 3 mM BPMA gels, despite the lower immunoprobe target signal with 12 mM DZMA gels. Additionally, our relative autofluorescence results demonstrate that the conjugated double bonds in benzophenone adequately absorb electrons to emit autofluorescence, particularly in the 488 nm and 532 nm laser channels, which corresponds to benzophenone and benzopinacol emission when activated by UV light.[13]

Utilizing diazirine hydrogels to quantify single-cell protein expression

Finally, we investigated diazirine protein capture and SNR with a more complex protein sample (*i.e.*, from single-cell lysate). We hypothesize that with equivalent protein capture to BPMA hydrogels, the lower background signal in DZMA gels would improve detection of low abundance protein targets from single cells. We performed size-based separation single-cell immunoblotting,[12,22] using the same PA concentration (8%T) for BPMA and DZMA hydrogels and sodium dodecyl sulfate (SDS) denaturing conditions. Compared to unmodified PA hydrogels, BPMA hydrogels have been shown to slow down protein electrophoretic migration due to smaller pore size.[23] However, an alternatively tetrazole-functionalized PA gel was

reported to have similar pore size to the unmodified PA gel[23] demonstrating that different hydrogel modifications have different impacts on the hydrogel matrix. Thus, we also investigated how diazirine functionalized gels would impact electrophoretic mobility for single-cell immunoblotting, using the same experimental conditions (lysis and electrophoresis buffers and time scales) for BPMA and DZMA hydrogels.

Following single-cell lysis, we immunoprobed for the protein target PTBP1, an abundantly expressed nuclear protein target that has been previously detected with high SNR in single-cell immunoblotting.[24,25] PTBP1 migrated 1.3$\times$ faster in DZMA gels (electrophoretic mobility (μ) = 0.0053 $\pm$ 0.0003 mm^2 V^{-1} s^{-1}, $n = 688$ cells across 5 devices) than in BPMA gels (μ = 0.0038 $\pm$ 0.0002 mm^2 V^{-1} s^{-1}, $n = 1322$ cells across 5 devices) ($p < 0.01$; Mann–Whitney U test) (Fig. 3D). PTBP1 protein peak widths (Fig. 3E) were also 1.1$\times$ wider in DZMA gels ($4\sigma = 207.4 \pm 33.3$ μm) than BPMA gels (189.3 $\pm$ 25.7 μm) ($p < 0.01$; Mann–Whitney U test). In addition, protein capture, measured by area under the curve (AUC) of the immunoprobed protein peak, and SNR in the DZMA gels was observed to be much lower, compared to protein peaks in BPMA gels (Fig. 3C). Protein signal (AUC) in 12 mM DZMA gels was significantly lower, only 15% of the protein signal measured in the 3 mM BPMA gels and SNR in DZMA gels was 20% of the SNR in BPMA gels (Fig. 3C) ($p < 0.01$; Mann–Whitney U test, $n = 5$ hydrogel devices). We probed for additional targets to confirm that lower signal and faster electromigration observations were consistent across multiple protein targets (ESI Fig. S2†).

Based on the higher protein electrophoretic mobility in DZMA gels, we posit that DZMA gels have a larger pore size compared to BPMA gels, resulting in faster protein electromigration. All three protein targets migrated faster in DZMA gels at similar relative rates compared to migration in BPMA gels. Furthermore, the larger protein peak widths in DZMA gels compared to BPMA gels also suggests larger pore size in DZMA gels, as larger pore size would result in greater diffusion and thus larger peaks widths. During the hydrogel fabrication, DZMA gels took longer (1.5 hours) to polymerize than the BPMA gels (15–20 min). We hypothesize that the slower polymerization rate of the DZMA gels indicates that the higher concentration of diazirine acts as a carbon radical trap that inhibits the complete gel polymerization reaction and results in larger pore sizes in the final hydrogel matrix. To test gel pore size, we measured the gel equilibrium swelling ratio of each functionalized hydrogel compared to a negative control gel in deionized water (ESI Fig. S3A†) and found that DZMA gels had significantly greater swelling compared to both BPMA and the negative control gel ($p < 0.01$ Kruskal–Wallis, Holm correction). Because gel swelling depends on both the pore size as well as any interactions between the hydrogel matrix and solvent,[26] we also measured the swelling ratio in a more polar solvent of 70% isopropyl alcohol (IPA) to better assess hydrogel hydrophobicity[27] (ESI Fig. S3B†). However, as PA is a hydrophilic polymer, the swelling ratios in 70% IPA were not significantly different between DZMA and BPMA gels. Thus,
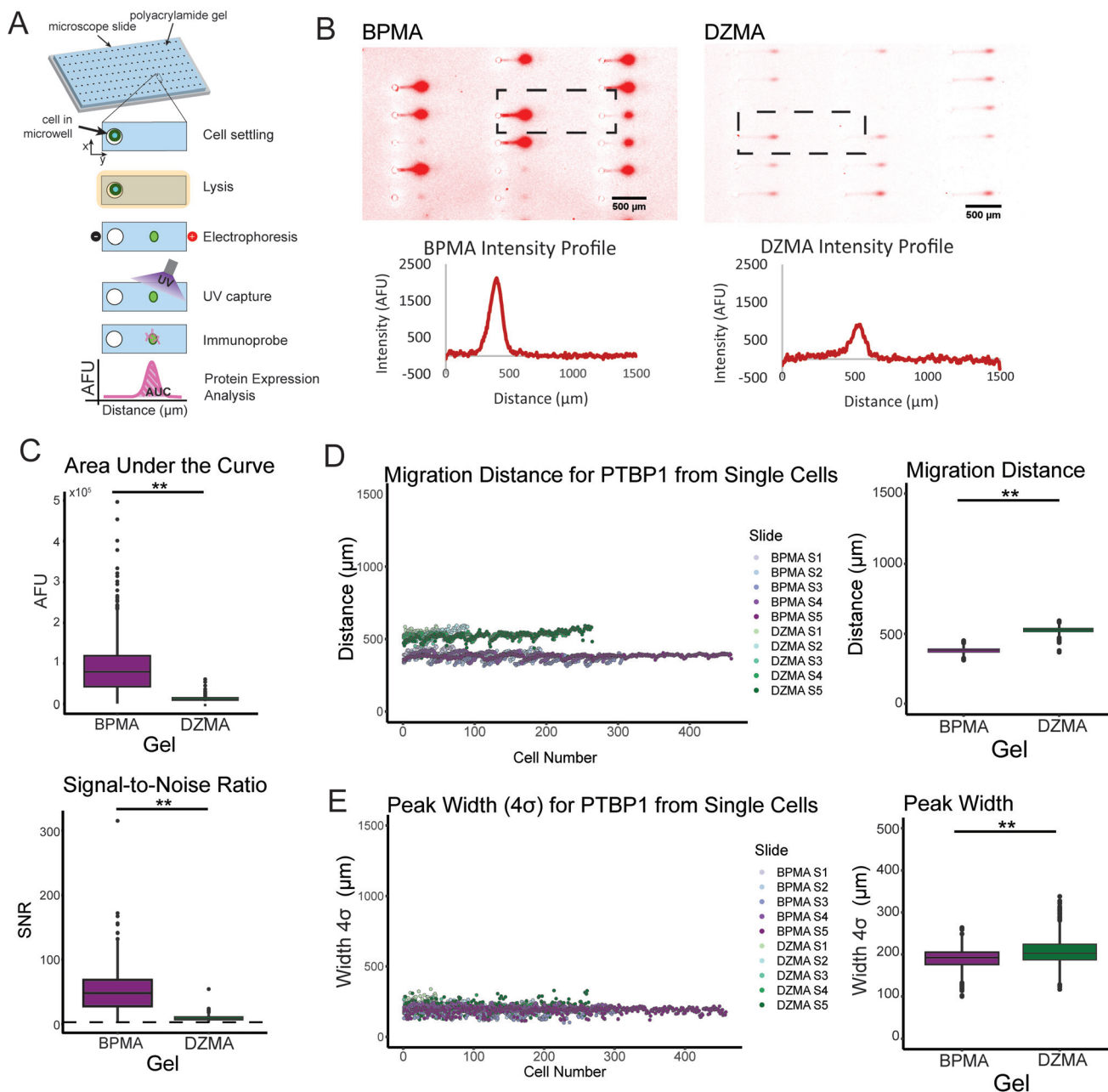
Fig. 3 Utilizing DZMA hydrogels for single-cell immunoblotting to detect PTBP1 (57 kDa) from MDA-MB-231 breast cancer cells. (A) Schematic of single-cell immunoblotting workflow: single-cells are gravity settled into an array of microwells for subsequent cell lysis and protein solubilization, protein PA gel electrophoresis, and in-gel immobilization of separated proteins. Protein targets are immunoprobed with fluorophore-conjugated antibodies. (B) Representative false-color fluorescence micrographs and intensity plots as examples of PTBP1 electromigration in each gel condition. (C) Analysis of PTBP1 area under the curve (AUC) signal and SNR following immunoprobing. The AUC and SNR is much higher in BPMA gels indicating higher protein capture efficiency. (D) Analysis of average peak migration distance for PTBP1 in a BPMA gel (purple) and DZMA gel (green) indicating faster protein migration in the DZMA gels. Each dot corresponds to a single-cell and each shade represents a distinct device (S1–S5 refer to device number). (E) Analysis of PTBP1 protein peak width (4σ) in both gels indicating slightly larger peak widths in DZMA gels. $N = 5$ replicate devices per gel condition, ** $p < 0.01$; Mann–Whitney U test.

the significantly higher swelling ratios of DZMA gels in water compared to BPMA hydrogels are more likely to indicate a larger pore size.

The lower signal following electrophoretic separations is unexpected when compared to the earlier protein incubation experiments. We investigated how the denatured protein structure would influence protein capture efficiency. Previously, it has been observed that benzophenone protein capture efficiency was significantly higher with denatured protein compared to native protein, likely due to greater exposure of hydro-

phobic residues that favor interaction with benzophenone.[28] Given the lower hydrophobicity of diazirine, the increased exposure of protein hydrophobic residues may result in less interaction with the diazirine molecule. To investigate the effect of protein structure, we ran native separations with fluorescently labelled purified protein diluted in 1× PBS and 1× Tris-glycine run buffer (non-denaturing conditions) and still observed higher AUC and SNR in 3 mM BPMA gels compared to 12 mM DZMA gels (ESI Fig. S4†), indicating that the denatured protein structure does not account for the difference in protein capture observed between the two experimental systems.

Conclusions

While photoactivatable protein crosslinking molecules are a critical way to functionalize hydrogels for immunoassay substrates, they can be sources of background fluorescence that impair immunoassay sensitivity. Here, we have determined that diazirine, which lacks conjugated double bonds, has significantly lower non-specific non-covalent interactions with fluorescent immunoprobes and significantly lower autofluorescence compared to benzophenone, resulting in overall lower in-gel immunoassay fluorescence background signal in DZMA hydrogels compared to BPMA-based hydrogels. However, when DZMA hydrogels were used for single-cell immunoblotting, the alternative diazirine chemistry resulted in faster protein electromigration and lower protein capture following the electrophoretic separations compared to BPMA gels, even though a higher concentration of diazirine capture molecules was utilized. Furthermore, increasing the concentration of DZMA appears to interfere with PA gel polymerization reaction, increasing polymerization completion times and affecting the gel pore size. We conclude that while diazirine has lower background signal, the lower capture efficiency and larger pore size of diazirine-modified hydrogels reduces its utility in open microfluidic systems susceptible to sample losses and does not effectively improve in-gel immunoassay sensitivity to detect low abundance protein targets.

Further investigation into other photoreactive molecules with higher protein capture efficiency than diazirines and lower background fluorescence than benzophenone may be of interest to functionalize hydrogels as immunoassay substrates. For example, aryl azides are another alternative photoreactive molecule used for protein crosslinking.[29] The singular aromatic ring on aryl azides may reduce the hydrophobicity and autofluorescence compared to the double aromatic rings on benzophenone.

Experimental

Antibodies

The primary antibodies to GFP (goat pAb; ab6673), β-tubulin (rabbit pAb; ab6046), and SFPQ (rabbit pAb; ab38148) were purchased from Abcam and the primary antibody to PTBP1

(mouse mAb; WH0005725M1) was purchased from Millipore Sigma. The secondary antibody to rabbit IgG pre-labelled with Alexa Fluor 647 (A31573) and mouse IgG pre-labelled with Alexa Fluor 555 (A31570) was purchased from Thermo Fisher Scientific. All primary antibodies were used at a 1 : 10 dilution from stock concentrations and incubated for 2 hours at room temperature. Secondary antibodies were diluted to a 1 : 20 working concentration from stock and incubated for 1 hour at room temperature, protected from light.

Chemicals

30%T, 3.3%C acrylamide/bis-acrylamide (29 : 1) (A3574), ammonium persulfate (APS, A3678), and tetramethyl-ethylene-diamine (TEMED, T9281) for gel polymerization, dichlorodi-methylsilane (440272) and 3-(trimethoxysilyl)propyl methacrylate (440159) for wafer and glass silanization, respectively, bovine serum albumin (BSA, A7638), fetal bovine serum (FBS, F2442), Triton X-100 (X100-100ML), and urea (U5378) were purchased from Sigma-Aldrich. Phosphate buffered saline (PBS, 10010023), RPMI 1640 medium (11875), penicillin–streptomycin (15070063) were purchased from Thermo Fisher Scientific. 1.5 M Tris-HCl, pH 8.8 (T1588) was purchased from Teknova, 10× Tris-glycine buffer (1610734) was purchased from Biorad, and 10× Tris buffered saline with Tween 20 (TBST, 9997S) was purchased from Cell Signaling Technologies. Deionized water (18.2 MΩ) was obtained using an Ultrapure water system from Millipore. N-[3-[(3-Benzoylphenyl)formamido]propyl]methacrylamide (BPMA) was custom synthesized by PharmAgra Laboratories.[12,22]

SU8 and polyacrylamide (PA) gel fabrication

SU8 fabrication to generate the master wafer and PA gel fabrication were performed as described previously.[12] Diazirine methacrylamide (DZMA) and N-[3-[(3-benzoylphenyl)forma-mido]propyl]meth-acrylamide (BPMA) were each solubilized in DMSO in a stock concentration before being added to the 8%T PA precursor in equal volumes. For the negative control, a blank vehicle control gel containing an equal volume of only DMSO was fabricated. Gels for protein capture and background fluorescence experiments were polymerized on a silanized glass slide using wafers (WaferPro C04009) microfabricated with SU-8 3050 (Kayaku Advanced Materials Y311075) to have ~40 μm "rails". Gels for single-cell immunoblotting were polymerized on a silanized glass slide using wafers (WaferPro C04009) microfabricated with SU-8 3050 (Kayaku Advanced Materials Y311075) to have 30 μm diameter "posts" to form microwells that were ~45 μm in height. All PA gel precursor was degassed and chemically polymerized with 0.08% APS and 0.08% TEMED. BPMA gels were polymerized for 15–20 minutes, covered and protected from light and DZMA gels were polymerized for 1.5 hours, covered and protected from light.

Protein and antibody labelling

His-tag green fluorescent protein (GFP) was labelled in-house with DyLight 633 using the described protocol in the DyLight

633 Antibody Labeling Kit, resulting in a degree-of-labelling of 0.46 fluorophores per molecule of protein. Anti-GFP primary antibody was labeled in-house using the described protocol in the Alexa Fluor 555 Antibody Labelling Kit, resulting in a degree-of-labeling of 4.16.

Evaluating diazirine methacrylamide protein capture

To quantify in-gel protein capture, we fabricated diazirine gels with increasing concentration of DZMA and used a gasket system (ArrayIt Microarray Gasket, ArrayIt Corporation, Sunnyvale, CA) to physically isolate regions of the gels and selectively incubate regions with a protein or blank solution as previously described.[30] Purified 0.01 mg mL^{-1} of His-GFP protein labeled in-house with DyLight 633 (DOL: 0.4–0.5) diluted in 1× PBS was loaded into pre-selected 1 cm × 1 cm regions while the remaining regions were loaded with 1× PBS buffer. After a 1 hour incubation, gels were exposed to colli-mated UV light under a mercury arc lamp (365 nm, at ~18.0 mW cm^{-2}, Optical Associates, Inc.) for 100 s to activate protein capture molecules to form covalent bonds with diazir-ine or benzophenone moieties and the protein species. Following UV exposure, gels were subsequently washed in 1× TBST before being dried with an N$_2$ stream and imaged on a microarray scanner using the 635 nm laser channel. After imaging on the laser microarray scanner, 6 ROIs with immobi-lized protein were measured for each replicate hydrogel and the integrated fluorescence intensity of each ROI was analyzed. Background subtraction was performed using the integrated fluorescence signal from an adjacent blank (no protein) region to account for any fluorescence signal from the hydrogel itself.

Evaluating antibody probe contribution to background fluorescence following in-gel immunoprobing

To assess background fluorescence from the antibody probe, 40 μm-thick hydrogels were fabricated for the endpoint range concentrations of DZMA (3 mM and 12 mM) to compare to a blank vehicle control and 3 mM BPMA positive control gel. Protein was loaded and captured into gels following the same protocol for evaluating DZMA protein capture. After dehydra-tion, gels were imaged using the 532 nm laser channel on the microarray scanner, corresponding to the immunoprobe fluorophore to obtain a "before immunoprobing" baseline measurement of the gel. After imaging, the gel was then rehy-drated in 1× TBST before immunprobing the entire gel (both protein and non-protein containing regions) by diffusing fluor-escently labelled anti-GFP primary antibody, labeled in-house with Alexa Fluor 555, into the PA gel. Gels were subsequently washed in 1× TBST to remove unbound antibody before being dried with an N$_2$ stream and re-imaged on a microarray scanner using the 532 nm laser channel with the same imaging settings to obtain an "after immunoprobing" measurement. The Immunoprobed Target Signal was quanti-fied as the integrated fluorescence signal from a protein region on the probed gel, using the integrated fluorescence signal from the same probed gel of an adjacent blank (non-protein) region for background subtraction. To measure the

Immunoprobed Background Signal, the integrated fluo-rescence signal from the blank region on the gel before immu-noprobing was subtracted from the integrated signal from the blank region on the gel after immunoprobing to account for any fluorescence signal from the gel itself.

Evaluating autofluorescence in BPMA and DZMA gels

40 μm-thick hydrogels were fabricated on silanized glass slides. Half of the bottom of the glass slide was covered with Kapton tape Electron Microscopy Sciences, 77708-02 and sur-rounded with aluminum foil to block any light from reaching the gel during the 100-second UV-exposure (365 nm, at ~18.0 mW cm^{-2}, Optical Associates, Inc.), which illuminates from below. The fluorescence signal of the half of the gel that was exposed to UV relative to the fluorescence of the non-UV exposed region was compared across conditions in all four laser channels of the microarray scanner (λ = 488, 532, 594, 635 nm).

Cell lines and cell harvesting

MDA-MB-231 cells were obtained from the American Type Culture Collection (ATCC) and authenticated (Promega). The MDA-MB-231 cell line was maintained in RPMI 1640 sup-plemented with 1% penicillin/streptomycin and 10% FBS. Cells were kept in a 37 °C incubator at 5% CO$_2$. For single-cell immunoblotting, cells were harvested using 0.05% Trypsin-EDTA (Gibco, 25300-054), and resuspended in 4 °C 1× PBS at a concentration of ~10^6 cells per mL.

Single-cell immunoblotting

Single-cell Immunoblotting was performed as described pre-viously.[22] Briefly, cells were pipetted over the PA gel and settled by gravity into the microwells patterned in the PA gel. 1% SDS with 8 M urea lysis buffer was heated in a water bath to 55 °C and was poured over the PA gel in order to simul-taneously lyse all the cells in the microwells for 30 seconds. An electric field (E = 40 V·cm^{-1}) was applied to inject and separate proteins for 25 seconds in the PA gel abutting the microwell. After separation, proteins were immobilized in the gel matrix *via* a 45-second exposure to UV light (Lightningcure LC5, Hamamatsu) which activated the benzophenone methacryla-mide or diazirine methacrylamide functional group (incorpor-ated during gel fabrication) to cross-link proteins to the gel matrix.[22] The UV light guide was held ~25 cm above the gel for all experiments. Immobilized proteins were probed in-gel by diffusing primary and fluorescently-labelled secondary anti-body probes into the PA gel. A fluorescence microarray scanner (Genepix 4300A, Molecular Devices) equipped with 4-laser lines (λ = 488, 532, 594, 635 nm) acquired fluorescence readout.

Immunoblot signal quantification and statistical analysis

The data sets reported here are available from the corres-ponding author on reasonable request. The images were first processed in Fiji[31,32] by applying a median filter using the "Remove Outliers" macro with a 2-pixel radius and a threshold

value of 50 AFU to remove punctate noise. Quantification of fluorescence signal from immunoblots was processed by in-house scripts written in MATLAB (R2018b) as previously described.[22] Gaussian curves were fit to fluorescence intensity profiles in MATLAB (R2018b, Curve Fitting Toolbox) in order to obtain the mean μ (used to describe the protein migration distance) and the variance σ^2 (used to calculate peak width as 4σ). Area under the curve (AUC) analysis of the intensity profiles was performed to quantify immunoblot signal 4σ from the fitted-curve peak location. The signal-to-noise ratio was calculated by taking the peak value of the Gaussian fit curve and dividing by the standard deviation of the background region from the 4σ region surrounding the peak. Only protein peaks with SNR $\geq$ 3 were included in downstream comparisons. Plots and statistical tests were generated and performed with R (version 3.6.1).

Author contributions

Conceived and designed the experiments: KYT, AEH, and SD. Synthesized diazirine methacrylamide: ER, CE. Performed the experiments: KYT. Analyzed the data: KYT. Contributed reagents/materials/analysis tools: SD, ER, CE, BW. Wrote the paper: KYT, SD, ER, CE, BW, and AEH.

Conflicts of interest

SD, ER, CE, and BW have a direct commercial affiliation to the funder of this study (Thermo Fisher Scientific). This affiliation provided funding and research materials for this study but did not affect the overall design and analysis of data or the decision to publish this manuscript. This study, or any of the materials included, are not related to any patents or products in development. Further, this affiliation also does not alter our adherence to Royal Society of Chemistry policies on sharing data and materials. AEH is a co-inventor on University of California intellectual property regarding single-cell immuno-blotting. KYT has no conflicts to disclose.

Acknowledgements

Notes and references

1 M. K. Gupta, J. R. Martin, B. R. Dollinger, M. E. Hattaway and C. L. Duvall, *Adv. Funct. Mater.*, 2017, **27**, 1–14.
2 R. Negishi, R. Iwata, T. Tanaka, D. Kisailus, Y. Maeda, T. Matsunaga and T. Yoshino, *Analyst*, 2019, **144**, 990–996.
3 I. Batalov, K. R. Stevens and C. A. DeForest, *Proc. Natl. Acad. Sci.*, 2021, **118**(4), DOI: 10.1073/pnas.2014194118.
4 Y. Ling, J. Rubin, Y. Deng, C. Huang, U. Demirci, J. M. Karp and A. Khademhosseini, *Lab Chip*, 2007, **7**, 756–762.
5 G. C. Le Goff, R. L. Srinivas, W. A. Hill and P. S. Doyle, *Eur. Polym. J.*, 2015, **72**, 386–412.
6 E. I. Dementieva, A. Y. Rubina, E. L. Darii, V. I. Dyukova, A. S. Zasedatelev, T. V. Osipova, T. P. Ryabykh, A. Y. Baryshnikov and A. D. Mirzabekov, *Dokl. Biochem. Biophys.*, 2004, **395**, 88–92.
7 D. Brambilla, M. Chiari, A. Gori and M. Cretich, *Analyst*, 2019, **144**, 5353–5367.
8 M. Sharafeldin, K. McCaffrey and J. F. Rusling, *Analyst*, 2019, **144**, 5108–5116.
9 D. A. Zubtsov, E. N. Savvateeva, A. Y. Rubina, S. V. Pan'kov, E. V. Konovalova, O. V. Moiseeva, V. R. Chechetkin and A. S. Zasedatelev, *Anal. Biochem.*, 2007, **368**, 205–213.
10 A. J. Hughes, R. K. C. Lin, D. M. Peehl and A. E. Herr, *Proc. Natl. Acad. Sci. U. S. A.*, 2012, **109**, 5972–5977.
11 G. Dormán, H. Nakamura, A. Pulsipher and G. D. Prestwich, *Chem. Rev.*, 2016, **116**, 15284–15398.
12 A. J. Hughes, D. P. Spelke, Z. Xu, C.-C. Kang, D. V. Schaffer and A. E. Herr, *Nat. Methods*, 2014, **11**, 749–755.
13 M. H. Schneider, Y. Tran and P. Tabeling, *Langmuir*, 2011, **27**, 1232–1240.
14 A. Su, B. E. Smith and A. E. Herr, *Anal. Chem.*, 2019, **92**, 875–883.
15 CSID:10629329, http://www.chemspider.com/Chemical-Structure.10629329.html, (accessed 20 June 2021).
16 CSID:2991, http://www.chemspider.com/Chemical-Structure.2991.html, (accessed 20 June 2021).
17 J. Brunner, H. Senn and F. M. Richards, *J. Biol. Chem.*, 1980, **255**, 3313–3318.
18 Y. Tanaka, M. R. Bond and J. J. Kohler, *Mol. Biosyst.*, 2008, **4**, 473–480.
19 S. A. Fleming, *Tetrahedron*, 1995, **51**, 12479–12520.
20 G. Dormán and G. D. Prestwich, *Biochemistry*, 1994, **33**, 5661–5673.
21 D. H. R. Barton, J. C. Jaszberenyi, E. A. Theodorakis and J. H. Reibenspies, *J. Am. Chem. Soc.*, 1993, **115**, 8050–8059.
22 C.-C. Kang, K. A. Yamauchi, J. Vlassakis, E. Sinkala, T. A. Duncombe and A. E. Herr, *Nat. Protoc.*, 2016, **11**, 1508–1530.
23 T. Zhang, S. Li, A. R. Warden, B. Ghalandari, H. Li and X. Zhi, *Adv. Funct. Mater.*, 2020, **1910739**, 1–8.

24 K. A. Yamauchi and A. E. Herr, *Microsyst. Nanoeng.*, 2017, **3**, 1–9.

25 K. Y. Tan and A. E. Herr, *Analyst*, 2020, **145**, 3732–3741.

26 S. H. Gehrke, J. P. Fisher, M. Palasis and M. E. Lund, *Ann. N. Y. Acad. Sci.*, 1997, **831**, 179–207.

27 D. J. Munoz-Pinto, B. Grigoryan, J. Long, M. Grunlan and M. S. Hahn, *J. Biomed. Mater. Res., Part A*, 2012, **100 A**, 2855–2860.

28 A. J. Hughes and A. E. Herr, *Proc. Natl. Acad. Sci. U. S. A.*, 2012, **109**, 21450–21455.

29 A. L. MacKinnon and J. Taunton, *Curr. Protoc. Chem. Biol.*, 2009, **1**, 55–73.

30 A. Gopal and A. E. Herr, *Sci. Rep.*, 2019, **9**, 1–12.

31 C. T. Rueden, J. Schindelin, M. C. Hiner, B. E. DeZonia, A. E. Walter, E. T. Arena and K. W. Eliceiri, *BMC Bioinf.*, 2017, **18**, 1–26.

32 J. Schindelin, I. Arganda-Carreras, E. Frise, V. Kaynig, M. Longair, T. Pietzsch, S. Preibisch, C. Rueden, S. Saalfeld, B. Schmid, J. Y. Tinevez, D. J. White, V. Hartenstein, K. Eliceiri, P. Tomancak and A. Cardona, *Nat. Methods*, 2012, **9**, 676–682.